Quantitative analysis of photon density of states for a realistic superlattice with omnidirectional light propagation

Ming-Chieh Lin[1,*] and Ruei-Fu Jao[1,2]
[1]*NanoScience Simulation Laboratory, Department of Physics, Fu Jen Catholic University, Taipei Hsien 24205, Taiwan, Republic of China*
[2]*Department of Physics, National Cheng Kung University, Tainan 701, Taiwan, Republic of China*
(Received 9 July 2006; revised manuscript received 8 August 2006; published 19 October 2006)

Omnidirectional light propagation in a realistic superlattice is investigated. This work complements two previous articles [Phys. Rev. E **59**, 3624 (1999); **61**, 5802 (2000)] that analyzed the cases of transverse electric (TE) and transverse magnetic (TM) polarization modes, respectively, of the dielectric superlattice modeled by means of Dirac δ functions. We present a quantitative analysis of the transmission functions, the band structures, the equifrequency surfaces, and the photon density of states (PDOS) for both TE and TM modes of the real superlattice without any approximations on the given dielectric function profiles. One of the advantages is that the Brewster effect can be manifested via our approach. In addition, the modes corresponding to TM evanescent waves that are absent from the Dirac comb model can be predicted. Finally, the exact PDOS of the realistic superlattice for the TE and TM modes can be obtained, respectively. These results are relevant to the spontaneous emission by an atom or to dipole radiation in one-dimensional periodic structures.

DOI: 10.1103/PhysRevE.74.046613 PACS number(s): 42.70.Qs, 42.25.Bs, 78.20.Bh

I. INTRODUCTION

In the past two decades, photonic crystals have attracted much attention [1]. To control the optical properties of materials has become a key issue in materials engineering. Many useful and interesting optical applications of thin films make use of multilayer stacks of films, or a superlattice (SL). To evaporate multiple layers while maintaining control over both refractive index and individual layer thickness has become a matured technology today [2]. Although a superlattice is a one-dimensional photonic crystal, it can exhibit three important characteristics of general photonic crystals including photonic band gaps, localized modes, and surface states. It is the simplest system for us to study new phenomena [3–8].

It was proposed that the emission of electromagnetic radiation can be modified by the environment [9,10]. Several environments such as metallic cavities [11], dielectric cavities [12], and superlattices [13–17] have been studied. In the case of the superlattices, the environmental effects have been described by the photon density of states (PDOS) for a superlattice. The PDOS is related to the transition rate of Fermi golden rule. There are many studies on the determination and analysis of the band gaps and the band structures. The PDOS for a superlattice modeled by means of a periodic array of Dirac δ functions, characterized by a grating parameter g has been studied [18–20]. The photon density of states as functions of frequency and the parameter g for both the transverse electric (TE) and transverse magnetic (TM) modes were obtained by making use of equifrequency surfaces in wave-vector space. Unfortunately, for this simple model, there is no manifestation of the Brewster effect in the band structure for the TM modes. Besides, this "Dirac comb" model was defined by means of a one-dimensional, periodic distribution of Dirac δ functions in a background dielectric medium and yielded a band structure that is similar to but not equal to that obtained from a realistic model of the superlattice. The model makes sense only if the dielectric constant of the barriers is large enough and its thickness is small enough. The PDOS calculated from this model will depart from that of a real superlattice for this reason.

In this work, omnidirectional light propagation in a realistic superlattice is investigated. The polarization characteristics including both the TE and TM modes are considered in our simulation model. A transfer-matrix approach is employed to discretize the dielectric function profile of the superlattice, and the transmission functions are calculated by matching the boundary conditions at each interface [2]. The corresponding band structures are obtained by solving the eigenvalue equations with proper periodic boundary conditions following the Bloch theorem [21,22]. The equifrequency surfaces in wave-vector space are employed to facilitate the calculation of the photon density of states. The photon densities of states of the superlattice for TE and TM modes are calculated, respectively. The contributions of the PDOS from the radiative and evanescent waves can be distinguished. The model is formulated in Sec. II. The calculated results and discussion are presented in Sec. III. The conclusions are given in Sec. IV.

II. FORMULATION

A. Transfer matrix method

All of macroscopic electromagnetism, including the propagation of light in a photonic crystal, is governed by the four macroscopic Maxwell's equations with no free charges or currents. For time-harmonic fields it is convenient to use a phasor notation. The Maxwell's equations lead to the wave equations, or the master equations:

*Also at Physics Division, National Center for Theoretical Science, Taiwan, ROC, as a visiting scientist. Electronic address: mclin@mails.fju.edu.tw

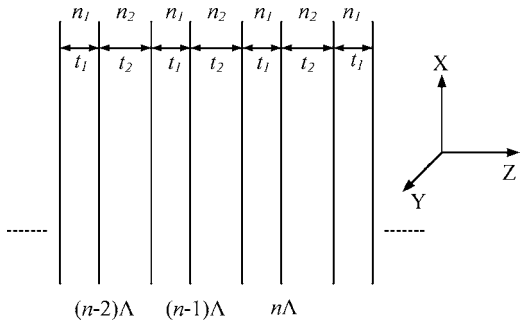

FIG. 1. Schematic of a realistic superlattice

$$\vec{\nabla} \times \left[\frac{1}{\mu(r)} \times \vec{\nabla} \times \vec{E}(r) \right] - \omega^2 \epsilon(r) \vec{E}(r) = \vec{0} \tag{1}$$

and

$$\vec{\nabla} \times \left[\frac{1}{\epsilon(r)} \times \vec{\nabla} \times \vec{H}(r) \right] - \omega^2 \mu(r) \vec{H}(r) = \vec{0}. \tag{2}$$

In a one-dimensional periodic system, the refractive index is a periodic function of z, as shown in Fig. 1. We assume that the materials are linear, homogeneous, isotropic, lossless, and nonmagnetic. We have

$$n(z) = \begin{cases} n_1, & 0 < z < t_1, \\ n_2, & t_1 < z < \Lambda, \end{cases} \tag{3}$$

where $n(z)=n(z+\Lambda)$ and Λ is the period. The dielectric function profile can be discretized by a transfer matrix method, and the two master equations are reduced to two homogeneous Helmholtz's equations for the pth region,

$$\nabla^2 \vec{E}_p(r) + k_0^2 n_p^2 \vec{E}_p(r) = \vec{0} \tag{4}$$

and

$$\nabla^2 \vec{H}_p(r) + k_0^2 n_p^2 \vec{H}_p(r) = \vec{0}. \tag{5}$$

For off-axis propagation, two polarizations, TE and TM modes, are both considered using Eqs. (4) and (5), respectively. The boundary conditions for the electric and magnetic fields of plane waves incident on the interfaces of p and $p+1$ layers are that the tangential components of the resultant E and H fields be continuous across the interface; that is, their magnitudes on either side must be equal. By matching the boundary conditions, we arrive at

$$\begin{pmatrix} E_{p-1} \\ H_{p-1} \end{pmatrix} = \begin{pmatrix} \cos \delta_p & i \sin \delta_p / \gamma_p \\ i \gamma_p \sin \delta_p & \cos \delta_p \end{pmatrix} \cdot \begin{pmatrix} E_p \\ H_p \end{pmatrix}, \tag{6}$$

where the δ's and γ's are defined as

$$\delta_p = k_0 \Delta_p = \frac{2\pi}{\lambda_0} n_p t_p \cos(\theta_{t_p}), \tag{7}$$

$$\gamma_p = \frac{n_p}{\mu_0} \sqrt{\epsilon_0 \mu_0} \cos \theta_{t_p} \text{ for the TE mode}, \tag{8}$$

and

$$\gamma_p = \frac{n_p}{\mu_0 \cos \theta_{t_p}} \sqrt{\epsilon_0 \mu_0} \text{ for the TM mode}. \tag{9}$$

In general, for a multilayer of arbitrary number N of layers,

$$\begin{pmatrix} E_{i0} + E_{r0} \\ \gamma_0 (E_{i0} - E_{r0}) \end{pmatrix} = m_1 m_2 m_3 \cdots m_N \begin{pmatrix} E_{t(N+1)} \\ \gamma_{N+1} E_{t(N+1)} \end{pmatrix}. \tag{10}$$

The 2×2 matrix is the overall transfer matrix of the film, represented by

$$m_T = \begin{pmatrix} m_{11} & m_{12} \\ m_{21} & m_{22} \end{pmatrix} = m_1 m_2 m_3 \cdots m_N. \tag{11}$$

Equation (10) can be solved for the transmission and reflection coefficients in terms of the transfer-matrix elements to give

$$t = \frac{2\gamma_0}{\gamma_0 m_{11} + \gamma_0 \gamma_{N+1} m_{12} + m_{21} + \gamma_{N+1} m_{22}} \tag{12}$$

and

$$r = \frac{\gamma_0 m_{11} + \gamma_0 \gamma_{N+1} m_{12} - m_{21} - \gamma_{N+1} m_{22}}{\gamma_0 m_{11} + \gamma_0 \gamma_{N+1} m_{12} + m_{21} + \gamma_{N+1} m_{22}}. \tag{13}$$

The transmittance and reflectance can be obtained via the following equations:

$$T = \frac{\gamma_{N+1}}{\gamma_0} t t^* \tag{14}$$

and

$$R = r r^*. \tag{15}$$

B. Band structure

For our periodic structure, the wave-vector component k_z is given by the Bloch vector k_B which may be restricted to the first Brillouin zone, $-\pi/\Lambda < k_B < \pi/\Lambda$. Because the dielectric function is independent of x and y, the electric field in the σ ($\sigma=1,2$) layer of the nth unit cell can be represented by

$$\vec{E}_{n,\sigma}(r) = [E^+_{n,\sigma} e^{-ik_{\sigma z}(z-n\Lambda)} + E^-_{n,\sigma} e^{ik_{\sigma z}(z-n\Lambda)}] e^{-i(k_x x + k_y y)} \hat{e_k}, \tag{16}$$

where

$$n\Lambda < z < (n+1)\Lambda, \tag{17}$$

$E^+_{n,\sigma}$ ($E^-_{n,\sigma}$) is the amplitude of the forward (backward) wave, and $\hat{e}_k$ is a unit vector with arbitrary direction in the xy plane. With $k_\parallel^2 = k_x^2 + k_y^2$,

$$k_{\sigma z} = \left[\left(\frac{n_\sigma \omega}{c} \right)^2 - k_\parallel^2 \right]^{1/2}. \tag{18}$$

According to the Bloch theorem, the electric and magnetic fields in a periodic layered medium are $E(z)=E(z+\Lambda)$ and $H(z)=H(z+\Lambda)$. The column vector of the Bloch wave satisfies the following eigenvalue equation:

$$\begin{pmatrix} E_0 \\ H_0 \end{pmatrix} = \begin{pmatrix} A & B \\ C & D \end{pmatrix} \begin{pmatrix} E_2 \\ H_2 \end{pmatrix} = e^{ik_B\Lambda} \begin{pmatrix} E_2 \\ H_2 \end{pmatrix}, \tag{19}$$

where E_0 and H_0 (E_2 and H_2) are the electric and magnetic fields at the left (right) boundary of the zeroth unit cell, respectively, and A, B, C, and D are

$$A = \cos\,\delta_1 \cos\,\delta_2 - \frac{\gamma_2 \sin\,\delta_1 \sin\,\delta_2}{\gamma_1}, \tag{20}$$

$$B = \frac{i \cos\,\delta_2 \sin\,\delta_1}{\gamma_1} + \frac{i \cos\,\delta_1 \sin\,\delta_2}{\gamma_2}, \tag{21}$$

$$C = i\gamma_1 \cos\,\delta_2 \sin\,\delta_1 + i\gamma_2 \cos\,\delta_1 \sin\,\delta_2, \tag{22}$$

and

$$D = \cos\,\delta_1 \cos\,\delta_2 - \frac{\gamma_1 \sin\,\delta_1 \sin\,\delta_2}{\gamma_2}. \tag{23}$$

The phase factor $e^{ik_B\Lambda}$ is thus the eigenvalue of the transfer matrix and satisfies the secular equation

$$\begin{vmatrix} A - e^{ik_B\Lambda} & B \\ C & D - e^{ik_B\Lambda} \end{vmatrix} = 0. \tag{24}$$

Finally, the dispersion relation between ω, k_y, and k_B for the Bloch wave function is

$$k_B(k_y,\omega) = \frac{1}{t_1 + t_2} \cos^{-1}\left[\frac{1}{2}(A + D)\right]. \tag{25}$$

C. Photon density of states

To perform the PDOS calculation, it is required to use its formal definition which is the number of available photon modes per unit frequency range. Then we construct two equifrequency surfaces: namely, $\omega(k_x,k_y,k_B)=\omega$ and $\omega(k_x,k_y,k_B)=\omega+\Delta\omega$, where $\Delta\omega$ is a small increment. We calculate the volume therein and divide it by the volume occupied by a single mode. The differential volume element in k space within the surfaces, as shown in Fig. 2, is given by

$$\Delta V_k = 2\pi k_\parallel \Delta\kappa_t \Delta\kappa_n, \tag{26}$$

where $\Delta\kappa_t = \sqrt{\Delta k_B^2 + \Delta k_\parallel^2}$ is a differential segment parallel to the equifrequency surface and $\Delta\kappa_n$ is the separation of the two surfaces that corresponds to the frequency increment. In order to obtain Eq. (26), it is necessary to rotate the area element $\Delta\kappa_t\Delta\kappa_n$ around the k_B axis. Here, $\Delta\kappa_n$ is perpendicular to the surface and defined as

$$\Delta\kappa_n = \frac{\Delta\omega}{|\nabla_k\omega|}. \tag{27}$$

Substituting Eq. (27) into Eq. (26) and integrating over the equifrequency surface, we have that the total phase-space volume contributing to the frequency range $(\omega,\omega+d\omega)$ as

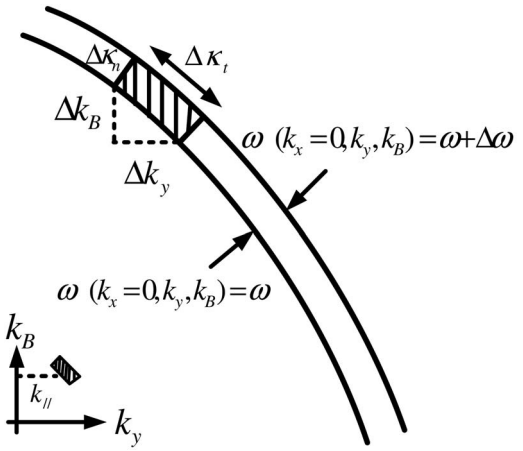

FIG. 2. Partial cross sections in the $k_x=0$ plane of two equifrequency surfaces denoted by ω and $\omega+\Delta\omega$. Using the azimuthal symmetry, the total volume element is $\Delta V_k = 2\pi k_\parallel \Delta\kappa_t \Delta\kappa_n$ and has the shape of a ring of a rectangular cross section.

$$\int_{\omega_k} dV_k = 2\pi d\omega \int_{\omega_k} \frac{k_\parallel}{|\nabla_k\omega|} d\kappa_t, \tag{28}$$

where we take the limit of infinitesimal increments. The number of modes within the range $(\omega,\omega+d\omega)$ is obtained from dividing the volume calculated in Eq. (28) by the volume corresponding to one mode, $(2\pi)^3/V$, where V is the volume of the system. This yields

$$dN(\omega) = \frac{V}{4\pi^2}\left[\int_{\omega_k} \frac{k_\parallel}{|\nabla_k\omega|} d\kappa_t\right] d\omega = D(\omega)d\omega. \tag{29}$$

Because ω is a function of $\boldsymbol{k}$, we can write

$$\nabla_k\omega = \frac{\partial\omega}{\partial k_x}\hat{x} + \frac{\partial\omega}{\partial k_y}\hat{y} + \frac{\partial\omega}{\partial k_B}\hat{z}. \tag{30}$$

By the use of Eqs. (18) and (25) we have that

$$\nabla_k\omega_{TE} = \frac{1}{2\psi_a - \psi_{b_1} - \psi_{b_2}} \times[(2\psi_c - \psi_{d_1} - \psi_{d_2})(k_x\hat{x} + k_y\hat{y}) - 2\Psi_{TE}\hat{z}] \tag{31}$$

and

$$\nabla_k\omega_{TM} = \frac{1}{2\phi_a - \phi_b - \phi_c} \times[(2\phi_d - \phi_e - \phi_f)(k_x\hat{x} + k_y\hat{y}) - 2\Psi_{TM}\hat{z}], \tag{32}$$

where the definitions of the functions ψ's, ϕ's, and Ψ's are given in the Appendix. Then, the final expressions for the PDOS corresponding to the TE and TM modes, respectively, are

$$D(\omega)_{TE} = \frac{V}{4\pi^2}\int_{\omega_k} d\kappa_t \frac{|2\psi_a - \psi_{b_1} - \psi_{b_2}|k_\parallel}{\sqrt{k_\parallel^2(2\psi_c - \psi_{d_1} - \psi_{d_2})^2 + 4\Psi_{TE}^2}} \tag{33}$$

and

$$D(\omega)_{TM} = \frac{V}{4\pi^2}\int_{\omega_k} d\kappa_t \frac{|2\phi_a - \phi_b - \phi_c|k_\parallel}{\sqrt{k_\parallel^2(2\phi_d - \phi_e - \phi_f)^2 + 4\Psi_{TM}^2}}. \tag{34}$$

III. RESULTS AND DISCUSSION

We consider the omnidirectional light propagation in an inhomogeneous, linear, and nonmagnetic medium, as shown in Fig. 1. The PDOS for a superlattice modeled by means of a periodic array of Dirac δ functions, characterized by a grating parameter g, has been studied [18–20]. The photon density of states as functions of frequency and the parameter g for both the TE and TM modes were obtained by making use of equifrequency surfaces in wave-vector space. This "Dirac comb" model was defined by means of a one-dimensional, periodic distribution of Dirac δ functions in a background dielectric medium. As a brief explanation of this Dirac comb model, we can say that it comes from considering a real superlattice, formed by an infinite array of alternating layers with dielectric constants ϵ_0 and ϵ_m whose widths are t_1 and t_2, respectively, and Λ is the period. If we take the limits $\epsilon_m \to \infty$ and $t_2 \to 0$ in such a way that the factor $\epsilon_m t_2/\Lambda$ is kept constant, then the Dirac δ model can be obtained. In this limit the factor $\epsilon_m t_2/\Lambda$ becomes the grating strength g. The dielectric function that can be found in the papers is given here for reference,

$$\epsilon(z) = \epsilon_0 + g\Lambda \sum_{N=-\infty}^{\infty} \delta(z - N\Lambda), \tag{35}$$

where

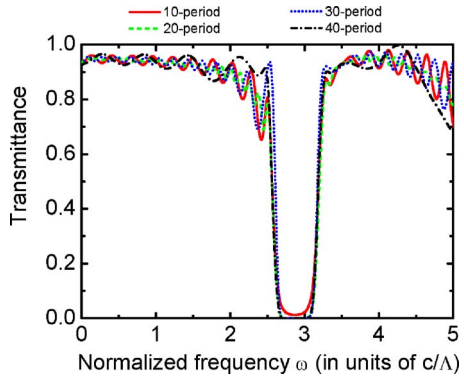

FIG. 3. (Color online) Calculated transmittance of the superlattice as a function of frequency for the cases of normal incidence with 10, 20, 30, and 40 periods. The refractive indices are $n_1=1$ and $n_2=\sqrt{3}$, and the corresponding thicknesses are $t_1=0.9\Lambda$ and $t_2=0.1\Lambda$.

$$g = (\epsilon_m - \epsilon_0)\frac{t_2}{\Lambda}. \tag{36}$$

Here, a realistic superlattice is investigated. A transfer-matrix approach is employed to discretize the dielectric function profile of the dielectric superlattice, and the transmission functions are calculated by matching the boundary conditions at each interface. Figure 3 shows our calculated transmittance as a function of frequency for the cases of normal incidence with 10, 20, 30, and 40 periods. The refractive indices are $n_1=1$ and $n_2=\sqrt{3}$, and the corresponding thicknesses are $t_1=0.9\Lambda$ and $t_2=0.1\Lambda$. The first forbidden gap can be determined to be in the range from 2.76 to 3.08 (in normalized frequency).

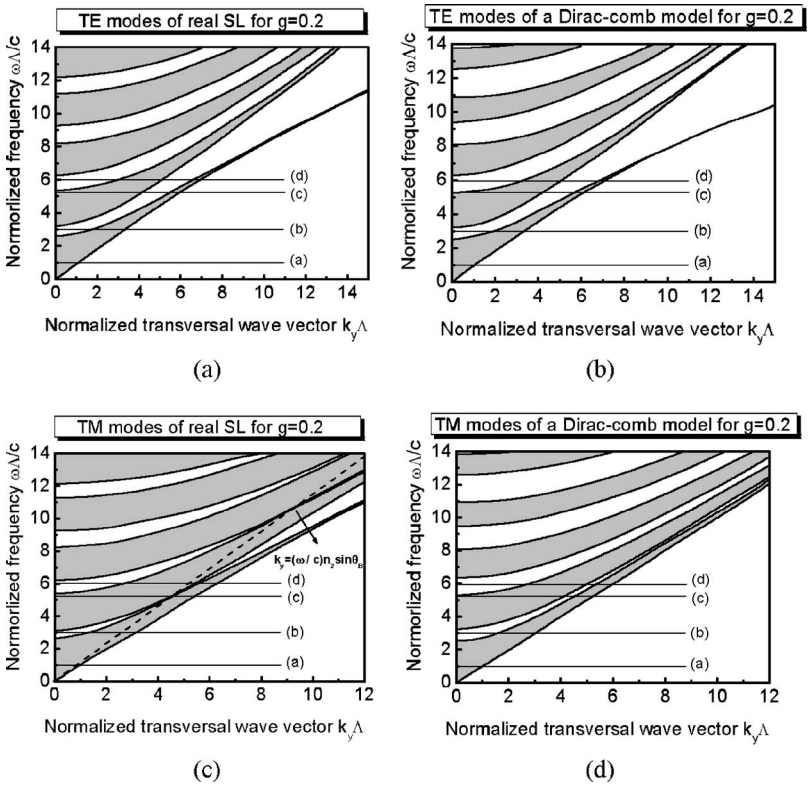

FIG. 4. Comparisons of the band structures of TE and TM modes of a real SL ($n_1=1$, $n_2=\sqrt{3}$, $t_1=0.9\Lambda$, and $t_2=0.1\Lambda$), (a) and (c), with that of the Dirac δ function model ($n_1=1$ and $g=0.2$), (b) and (d).

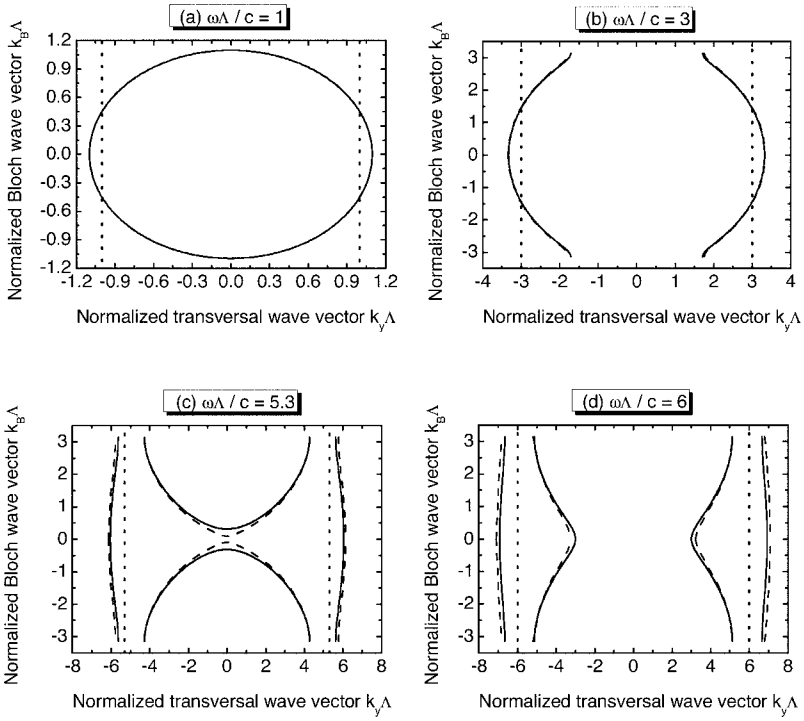

FIG. 5. Four cross sections ($k_x=0$) of the equifrequency surfaces of TE modes $\omega(k_x,k_y,k_B)=\omega=$const for $g=0.2$. The solid lines and the dashed lines correspond to the real SL model and the Dirac comb model, respectively. The dotted lines denote $|k_y|=\omega n_1/c$, so that the region between (outside) these lines is characterized by real (imaginary) k_z values.

The corresponding band structures are obtained by solving the eigenvalue equations with proper periodic boundary conditions as following the Bloch theorem. The band structures of TE and TM modes, by solving Eq. (25), for the special case are plotted in Figs. 4(a) and 4(c), respectively.

Our method has been checked by comparing with the limiting case, the Dirac δ function model with $g=0.2$. The corresponding band structures are plotted in Figs. 4(b) and 4(d). The shadowed regions are the allowed bands, and all the band edges are characterized by $\cos(k_B\Lambda)=\pm 1$. One can see the differences between these two approaches. It is clear that the Dirac comb model cannot give rise to the Brewster effect for the TM modes and, indeed, no closure of the band gaps is manifested in Fig. 4(d). On the other hand, the realistic method predicts a distinctive feature for the TM modes: namely, the closure of the band gaps alongside a straight line through the origin. In Fig. 4(c), the forbidden bands shrink to zero when $k_y=(\omega/c)n_2 \sin\theta_B$ with θ_B the Brewster angle, known as the Brewster's condition. One of the advantages is that the Brewster effect can be manifested in our approach.

The equifrequency surfaces in wave-vector space are employed to facilitate the calculation of the photon densities of

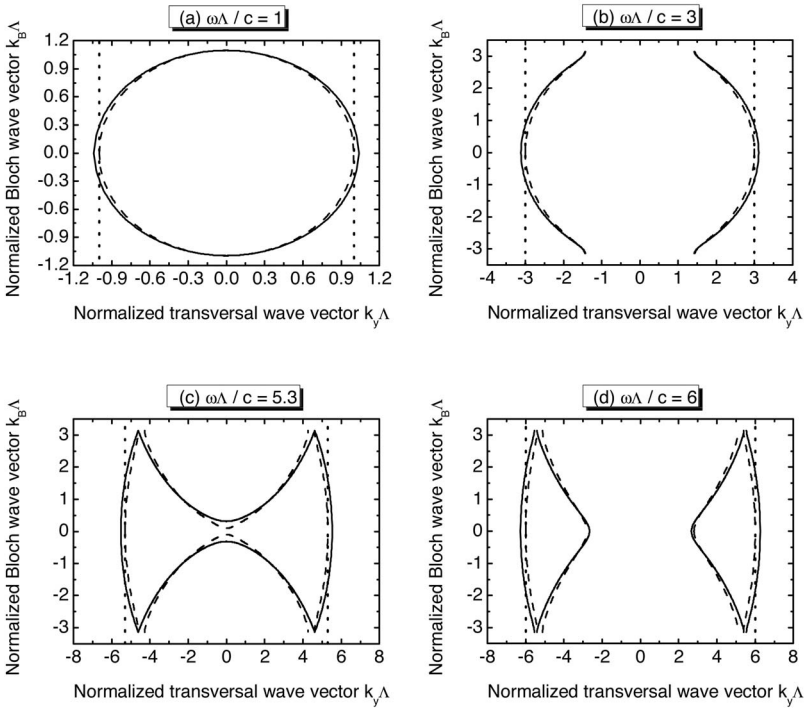

FIG. 6. Four cross sections ($k_x=0$) of the equifrequency surfaces of TM modes $\omega(k_x,k_y,k_B)=\omega=$const for $g=0.2$. The solid lines and the dashed lines correspond to the real SL model and the Dirac comb model, respectively. The dotted lines denote $|k_y|=\omega n_1/c$, so that the region between (outside) these lines is characterized by real (imaginary) k_z values.

states. The photon densities of states of the superlattice for TE and TM modes are calculated, respectively. In Figs. 5 and 6, several $\omega(k_x,k_y,k_B)$=const curves for the TE and TM modes in solid lines are sketched in two-dimensional plots, respectively. Due to the azimuthal symmetry of the problem, we can obtain the three-dimensional equifrequency surface $\omega(k_x,k_y,k_B)$=const simply by rotating the curves around the k_B axis. To describe the surfaces depicted in Figs. 5 and 6, look at the band structure in Fig. 4. In this figure, horizontal lines are drawn at the frequency values selected in Figs. 5(a) and 6(a), 5(b) and 6(b), 5(c) and 6(c), 5(d) and 6(d). Line (a) lies entirely within the lowest allowed band, so that the equifrequency surface is closed. Line (b), corresponding to a greater frequency, lies in part in the first band gap and in part in the first band. This produces an interruption in the corresponding equifrequency surface for values $k_{\|}\Lambda<1$, as no solutions for the field exist therein. As the frequency keeps increasing, the line $\omega(k_x,k_y,k_B)$=const cuts through more and more passbands, so that the equifrequency surfaces split into several sections. This can be seen from Figs. 5(c), 5(d), 6(c), and 6(d) with the aid of the corresponding frequency lines transversing the band structure.

These surfaces grow in size with the frequency, as we can see from the $k_{\|}$ range for each value of the frequency. The curves corresponding to the limiting case for the Dirac δ function model with $g=0.2$ are also plotted as dashed lines for comparisons. The dotted lines denote $|k_y|=\omega n_1/c$. Notice that $k_{\|}$ can exceed the value of $\omega n_1/c$. The modes located in that part of the surface correspond to the case of imaginary k_z, and hence to evanescent waves, in the regions between the dielectric barriers. The Dirac comb model predicted that k_z can never be imaginary in the case of TM polarization. However, as one can see from Fig. 6, the modes corresponding to TM evanescent waves do exist, as predicted by our realistic method. In order to study the Brewster effect, we can cut the equifrequency surface at which the forbidden bands shrink to zero; we select the $\omega=5.3$ and the equifrequency surface as shown in Fig. 6(c). One can see the differences between the results of our realistic approach and that of the Dirac comb model. The only significant difference between the equifrequency surfaces for the realistic and Dirac comb models occurs for the case (c), in the region where both wave-vector components are very small. This occurs because in this case the frequency happens to be just inside (outside) the second band in Fig. 4 for the realistic (Dirac comb) model. Given the choice of the dielectric constant in the thin layers—only 3—the Dirac comb model works unexpectedly well. (It is supposed to work well only if there is a very large dielectric contrast between the layers.) We plot the PDOS for TE and TM modes in Figs. 7(a) and 7(b), respectively. It is seen that there are slope discontinuities. These slope discontinuities arise from the band gaps of the band structure. In the figure, an increment of the PDOS relative to free space is present for all frequencies and is particularly pronounced for frequencies near the lower edges of the band gaps. As a consequence, the PDOS never vanishes, as occurs if the wave is restricted to propagate along the axis of the superlattice. This value of $g=0.2$ corresponds to a weak modulation of the dielectric constant, so that the PDOS curves lie quite close to that of the free-space PDOS.

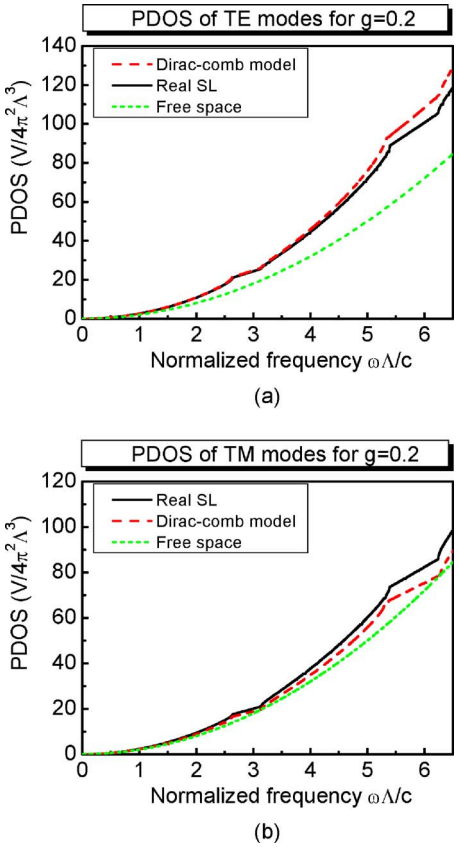

FIG. 7. (Color online) PDOS of TE modes (a) and TM modes (b) for $g=0.2$. The solid line and the dashed line correspond to the real SL model and the Dirac comb function model, respectively.

For such a small modulation of dielectric constants, we can still obtain the discrepancies in PDOS for the realistic approach and the Dirac comb model, as one can see in the figure. The Dirac δ function model is expected to give reasonable results for the PDOS qualitatively. However, for the quantitative analysis of a real superlattice, it is much better to employ this realistic method.

Figure 8 shows the PDOS normalized to that of the vacuum for the TE and TM modes for the same case. The normalized PDOS for the radiative and evanescent waves are also plotted. As one can see, although the PDOS for the TE and TM modes exhibit similar behavior, the corresponding contributions from the radiative and evanescent parts are quite different. For understanding spontaneous emission or dipole radiation in a realistic superlattice, one should consider both the TE and TM modes. So the total PDOS should be considered. We believe these results are relevant to the spontaneous emission by an atom or to dipole radiation in one-dimensional periodic structures. Realistic analysis of the problem can be done with our method.

Recently, the spontaneous emission of an atom embedded in a realistic superlattice has been studied [16,17]. It was found that the rate of emission presents a strong dependence on the atom's position. In addition, the emission spectrum shows an oscillatory behavior which follows the photonic band structure and the evanescent contribution to the spontaneous emission is dominant if a dielectric layer is in the

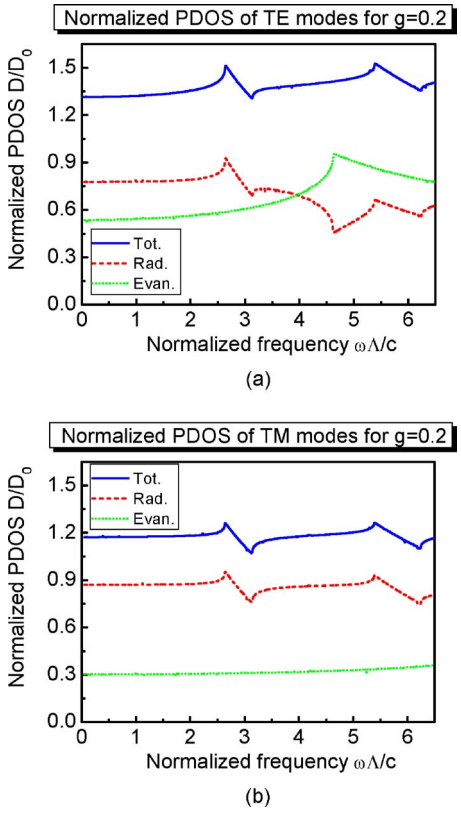

FIG. 8. (Color online) PDOS normalized to that of the vacuum for (a) TE and (b) TM modes. The dashed (dotted) lines correspond to the normalized PDOS of radiative (evanescent) waves.

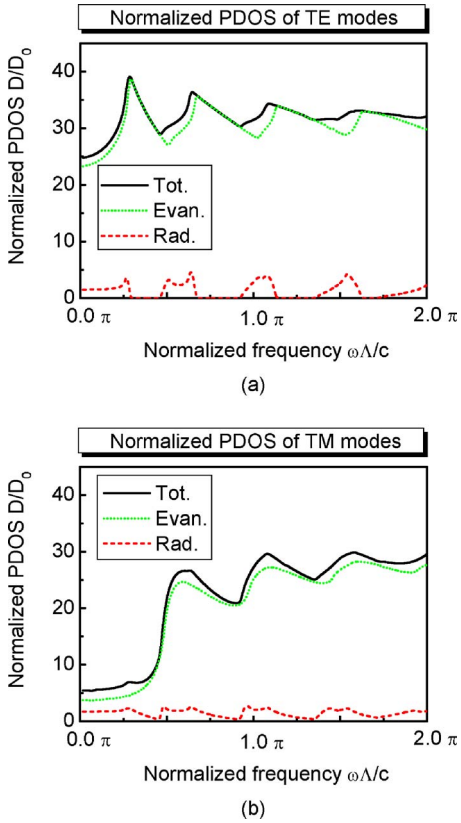

FIG. 9. (Color online) PDOS normalized to that of the vacuum for (a) TE and (b) TM modes with $t_1=t_2=\Lambda/2$, $n_1=1$, and $n_2=4$. The dashed (dotted) lines correspond to the normalized PDOS of radiative (evanescent) waves.

near field region of the dipole. Figure 9 shows our calculated PDOS normalized to that of the vacuum, D_0, for the TE and TM modes in the superlattice with $t_1=t_2=\Lambda/2$, $n_1=1$, and $n_2=4$, the same parameters as those in Ref. [16]. One can compare Figs. 9(a) and 9(b) in this paper with Figs. 2(c) and 4(c) in Ref. [16], respectively, to see they are quite similar. In these cases, the dielectric layer is in the near-field region of the atom, and the normalized rates of emission from the contributions of the radiative and evanescent waves, respectively, in Ref. [16] are characterized by the corresponding PDOS in this paper. As one can see from Fig. 9, the PDOS corresponding to the evanescent waves is much larger than that of the radiative waves for both the TE and TM modes. In the near-field region, the evanescent waves could be excited, especially for the TM modes, so that the evanescent contribution to the emission rate can be greatly enhanced due to the larger PDOS. This is consistent with the results of Ref. [16]. We relate our results to these articles and it is found that explicit computations of the PDOS could facilitate the understanding of these studies.

IV. CONCLUSIONS

In this work, omnidirectional light propagation in a realistic superlattice is investigated. The polarization characteristics including both the TE and TM modes are considered. A transfer-matrix approach is employed to discretize the dielectric function profile of the superlattice, and the transmission functions are calculated by matching the boundary conditions at each interface. The corresponding band structures are obtained by solving the eigenvalue equations with proper periodic boundary conditions following the Bloch theorem. The equifrequency surfaces in wave-vector space are employed to facilitate the calculation of the photon densities of states. The photon densities of states of the superlattice for TE and TM modes are calculated, respectively. Our method has been checked by comparing with the limiting case, the Dirac δ function model with $g=0.2$, giving good agreement. The realistic model of the superlattice predicts a distinctive feature for the TM modes: namely, the closure of the band gaps alongside a straight line through the origin. One of the advantages is that the Brewster effect can be manifested in our approach. In addition, the modes corresponding to TM evanescent waves that are absent from the Dirac comb model can be predicted by our method. For a small modulation of dielectric constants, we can still see the discrepancies in PDOS for the realistic approach and the Dirac comb model. The Dirac δ function model is expected to give reasonable results for the PDOS qualitatively. However, for the quantitative analysis of a real superlattice, it is much better to employ this realistic method. This work not only complements the previous 2 studies [18,19] but also facilitates the understanding of the third one [16]. We believe these results are relevant to the spontaneous emission by an atom or to dipole radiation in one-dimensional periodic structures.

ACKNOWLEDGMENTS

This work was partially supported by the National Science Council, Taiwan, ROC, under Grant No. NSC 95-2112-M-030-002, National Center for Theoretical Sciences, and National Center for High-Performance Computing, Taiwan, ROC, which provides the computing resources.

APPENDIX: FORMULAS

Here, we give the definitions of the functions employed in Eqs. (31)–(34)

$$\psi_a = \cos\,\delta_2 \sin\,\delta_1\left(-t_1\gamma_1 - \frac{k_\parallel^2 t_1}{\gamma_1\omega^2}\right) + \cos\,\delta_1 \sin\,\delta_2\left(-t_2\gamma_2 - \frac{k_\parallel^2 t_2}{\gamma_2\omega^2}\right), \tag{A1}$$

$$\psi_{b_1} = \left(\frac{\gamma_1}{\gamma_2} + \frac{\gamma_2}{\gamma_1}\right)\left[\cos\,\delta_1 \sin\,\delta_2\left(t_1\gamma_1 + \frac{k_\parallel^2 t_1}{\gamma_1\omega^2}\right) + \cos\,\delta_2 \sin\,\delta_1\left(t_2\gamma_2 + \frac{k_\parallel^2 t_2}{\gamma_2\omega^2}\right)\right], \tag{A2}$$

$$\psi_{b_2} = \frac{k_\parallel^2}{\omega^3}\sin\,\delta_1 \sin\,\delta_2\left(\frac{2}{\gamma_1\gamma_2} - \frac{\gamma_1}{\gamma_2^3} - \frac{\gamma_2}{\gamma_1^3}\right), \tag{A3}$$

$$\psi_c = \frac{1}{\omega}\left(\frac{t_1\cos\,\delta_2 \sin\,\delta_1}{\gamma_1} + \frac{t_2\cos\,\delta_1 \sin\,\delta_2}{\gamma_2}\right), \tag{A4}$$

$$\psi_{d_1} = -\frac{1}{\omega}\left[\cos\,\delta_1 \sin\,\delta_2\left(\frac{t_1\gamma_2}{\gamma_1^2} + \frac{t_1}{\gamma_2}\right) + \cos\,\delta_2 \sin\,\delta_1\left(\frac{t_2\gamma_1}{\gamma_2^2} + \frac{t_2}{\gamma_1}\right)\right], \tag{A5}$$

$$\psi_{d_2} = \frac{1}{\omega^2}\sin\,\delta_1 \sin\,\delta_2\left[\frac{1}{\gamma_1}\left(\frac{\gamma_2}{\gamma_1^2} - \frac{1}{\gamma_2}\right) + \frac{1}{\gamma_2}\left(\frac{\gamma_1}{\gamma_2^2} - \frac{1}{\gamma_1}\right)\right], \tag{A6}$$

$$\phi_a = \cos\,\delta_2 \sin\,\delta_1\left(-\frac{n_1^2 t_1}{\gamma_1} - \frac{k_\parallel^2 t_1\gamma_1}{n_1^2\omega^2}\right) + \cos\,\delta_1 \sin\,\delta_2\left(-\frac{n_2^2 t_2}{\gamma_2} - \frac{k_\parallel^2 t_2\gamma_2}{n_2^2\omega^2}\right), \tag{A7}$$

$$\phi_b = \left(\frac{\gamma_1}{\gamma_2} + \frac{\gamma_2}{\gamma_1}\right)\left[t_1\cos\,\delta_1 \sin\,\delta_2\left(\frac{n_1^2}{\gamma_1} + \frac{k_\parallel^2\gamma_1}{n_1^2\omega^2}\right) + t_2\cos\,\delta_2 \sin\,\delta_1\left(\frac{n_2^2}{\gamma_2} + \frac{k_\parallel^2\gamma_2}{n_2^2\omega^2}\right)\right], \tag{A8}$$

$$\phi_c = \frac{k_\parallel^2 \sin\,\delta_1 \sin\,\delta_2}{\omega^3}\left[\gamma_1\gamma_2\left(\frac{1}{n_1^4} + \frac{1}{n_2^4}\right) - \frac{\gamma_1^3}{n_1^4\gamma_2} - \frac{\gamma_2^3}{n_2^4\gamma_1}\right], \tag{A9}$$

$$\phi_d = \frac{1}{\omega}\left(\frac{t_1\gamma_1\cos\,\delta_2 \sin\,\delta_1}{n_1^2} + \frac{t_2\gamma_2\cos\,\delta_1 \sin\,\delta_2}{n_2^2}\right), \tag{A10}$$

$$\phi_e = -\frac{1}{\omega}\left[\frac{\cos\,\delta_1 \sin\,\delta_2}{n_1^2}\left(\frac{t_1\gamma_1^2}{\gamma_2} + t_1\gamma_2\right) + \frac{\cos\,\delta_2 \sin\,\delta_1}{n_2^2} \times\left(\frac{t_2\gamma_2^2}{\gamma_1} + t_2\gamma_1\right)\right], \tag{A11}$$

$$\phi_f = \frac{\sin\,\delta_1 \sin\,\delta_2}{\omega^2}\left[\frac{\gamma_1}{n_1^4}\left(\frac{\gamma_1^2}{\gamma_2} - \gamma_2\right) + \frac{\gamma_2}{n_2^4}\left(\frac{\gamma_2^2}{\gamma_1} - \gamma_1\right)\right], \tag{A12}$$

and

$$\Psi_{TE/TM} = (t_1 + t_2)\sqrt{1 - \frac{1}{4}\left[2\cos\,\delta_1\cos\,\delta_2 - \sin\,\delta_1 \sin\,\delta_2\left(\frac{\gamma_1}{\gamma_2} + \frac{\gamma_2}{\gamma_1}\right)\right]^2}. \tag{A13}$$

[1] J. D. Joannopoulos, R. D. Meade, and J. J. Winn, *Photonic Crystals: Molding the Flow of Light* (Princeton University Press, Princeton, 1995).

[2] F. L. Pedrotti and L. S. Pedrotti, *Introduction to Optics*, 2nd ed. (Prentice-Hall, Englewood Cliffs, NJ, 1993).

[3] R. J. Glauber and M. Lewenstein, Phys. Rev. A **43**, 467 (1991).

[4] M. Scalora, J. P. Dowling, A. S. Manka, C. M. Bowden, and J. W. Haus, Phys. Rev. A **52**, 726 (1995).

[5] M. Scalora, R. J. Flynn, S. B. Reinhardt, R. L. Fork, M. J. Bloemer, M. D. Tocci, C. M. Bowden, H. S. Ledbetter, J. M. Bendickson, J. P. Dowling, and R. P. Leavitt, Phys. Rev. E **54**, R1078 (1996).

[6] M. Scalora, M. J. Bloemer, A. S. Manka, J. P. Dowling, C. M. Bowden, R. Viswanathan, and J. W. Haus, Phys. Rev. A **56**, 3166 (1997).

[7] M. D. Tocci, M. Scalora, M. J. Bloemer, J. P. Dowling, and C. M. Bowden, Phys. Rev. A **53**, 2799 (1996).

[8] F. Ramos-Mendieta and P. Halevi, Opt. Commun. **129**, 1 (1996).

[9] E. M. Purcell, Phys. Rev. **69**, 681 (1946).
[10] D. Kleppner, Phys. Rev. Lett. **47**, 233 (1981).
[11] A. O. Barut and J. P. Dowling, Phys. Rev. A **36**, 649 (1987).
[12] H. Rigneault and S. Monneret, Phys. Rev. A **54**, 2356 (1996).
[13] J. P. Dowling and C. M. Bowden, Phys. Rev. A **46**, 612 (1992).
[14] T. Suzuki and P. K. L. Yu, J. Opt. Soc. Am. B **12**, 570 (1995).
[15] A. Kamli, M. Babiker, A. Al-Hajry, and N. Enfati, Phys. Rev. A **55**, 1454 (1997).
[16] A. S. Sánchez and P. Halevi, Phys. Rev. E **72**, 056609 (2005).
[17] P. Halevi and A. S. Sánchez, Opt. Commun. **251**, 109 (2005).
[18] I. Alvarado-Rodríguez, P. Halevi, and J. J. Sánchez-Mondragón, Phys. Rev. E **59**, 3624 (1999).
[19] J. R. Zurita-Sánchez and P. Halevi, Phys. Rev. E **61**, 5802 (2000).
[20] J. M. Bendickson, J. P. Dowling, and M. Scalora, Phys. Rev. E **53**, 4107 (1996).
[21] A. Yariv and P. Yeh, *Optical Waves in Crystals* (Wiley, New York, 1984).
[22] C. Kittel, *Introduction to Solid State Physics* (Wiley, New York, 1976).